

# Does Gaussian Splatting need SFM Initialization?

Yalda Foroutan<sup>1</sup>Daniel Rebain<sup>2</sup>Kwang Moo Yi<sup>2</sup>Andrea Tagliasacchi<sup>1,3,4</sup><sup>1</sup>Simon Fraser University, <sup>2</sup>University of British Columbia, <sup>3</sup>University of Toronto, <sup>4</sup>Google DeepMind

Figure 1. COLMAP [25, 26] (Left) vs. NeRF-based (Right) initialization point clouds for Gaussian Splatting. The NeRF-based initialization provides a much more complete model of the scene structure, while also being faster to construct with posed images.

## Abstract

3D Gaussian Splatting has recently been embraced as a versatile and effective method for scene reconstruction and novel view synthesis, owing to its high-quality results and compatibility with hardware rasterization. Despite its advantages, Gaussian Splatting’s reliance on high-quality point cloud initialization by Structure-from-Motion (SfM) algorithms is a significant limitation to be overcome. To this end, we investigate various initialization strategies for Gaussian Splatting and delve into how volumetric reconstructions from Neural Radiance Fields (NeRF) can be utilized to bypass the dependency on SfM data. Our findings demonstrate that random initialization can perform much better if carefully designed and that by employing a combination of improved initialization strategies and structure distillation from low-cost NeRF models, it is possible to achieve equivalent results, or at times even superior, to those obtained from SfM initialization.

## 1. Introduction

In the years since their introduction, Neural Radiance Fields (NeRF) [17] have emerged as a leading technique for 3D reconstruction from images and novel view synthesis, capturing the interest of researchers and practitioners alike. Despite its success, the application of NeRF in practical scenarios has

been limited by its high computational demands. Due in part to this limitation, 3D Gaussian Splatting [9] has gained traction as a more efficient alternative, as it achieves real-time inference speeds by leveraging hardware rasterization.

However, the adoption of Gaussian Splatting is not without challenges. A significant hurdle is its dependence on careful initialization from point clouds, such as those from Structure-from-Motion (SfM).

The reliance on slow and computationally expensive SfM implementations such as COLMAP [25, 26], and comparatively poor performance of random initialization is a critical limitation that impedes the application of Gaussian Splatting in domains where a full SfM solution would be too expensive. This includes situations like SLAM sequences where accurate camera poses are available alongside point clouds too sparse to be useful for initialization, such as ORB-SLAM [19], or autonomous vehicle applications where navigation and localization are performed with other sensors, e.g., aircraft.

Such applications could benefit significantly from a computationally efficient alternative to SfM for Gaussian Splatting initialization. With this motivation, our purpose in this work is to perform a deeper analysis of the initialization phase of Gaussian Splatting, and identify how existing methods could be leveraged to improve the situation.

We hypothesize that the limitations of Gaussian Splatting stem from its discrete and localized pruning and growing

operations, which struggle to capture the coarse structure of scenes effectively. In particular, regions of missing geometry in the SFM solution, such as those shown in Figure 1, which can be caused by lack of texture, dynamic scene content, or strong view-dependent effects, can leave the optimization near pathological minima which the local optimization fails to escape. In contrast, NeRF optimization handles such non-idealities more gracefully, tending to produce over-smoothed reconstructions rather than missing geometry.

Given the proficiency of NeRF and similar neural field-based volume-rendering methods in reconstructing scene geometry at a coarse level, our analysis centers on integrating these techniques into the Gaussian Splatting training pipeline. Specifically, we investigate both point cloud initialization and depth supervision derived from a NeRF model trained for a short amount of time on the same data.

**Contributions.** Through extensive experiments, we find that a combination of better random initialization and structure guidance from NeRF are sufficient to match or exceed the quality reached from a COLMAP initialization, even on very large-scale, challenging scenes. This result could have significant implications for applications of Gaussian Splatting which do not require an SFM solution to estimate camera poses, such as autonomous vehicles with fused inertial/satellite navigation, or for which SFM solutions are not reliable. We also find that the required training time for the NeRF teacher model can be very low, on the order of 30 seconds – much faster than large SFM reconstructions, and even the Gaussian Splatting training itself.

## 2. Related Work

**Differentiable rendering architectures.** Since the introduction of neural fields [4, 16, 22], a variety of neural rendering methods have been proposed which use gradient descent optimization of image reconstruction objectives to construct scene representations for novel view synthesis. Perhaps most notable is Neural Radiance Fields (NeRF) [17], which has become the basis of an ever-expanding family of volumetric scene models. While NeRF originally used a purely neural model, further works explored methods based partially [14] or entirely [6] on classical grids as a way of exploring the trade-off between compactness and efficiency.

**Accelerated volumetric rendering.** As it became clear that much higher efficiency could be achieved through application of grid structures, works like Instant Neural Graphics Primitives (INGP) [18] and Tensorial Radiance Fields (TensorRF) [3] appeared which leveraged not only grid structures but additional strategies of hashing and tensor factorization to compress the grid representation itself, leading to significant gains in both training and inference speed.

**Gaussian Splatting.** While significant advances have been

made in improving the efficiency of models based on volume rendering, it is still a challenge to reach truly interactive inference speeds with them, due largely to the Monte Carlo integration required for each ray. An alternative approach to differentiable rendering that avoids this is *rasterization*, in which individual primitives are projected into image space and written to a buffer in order of depth. One such method is Pulsar [12], which uses partially transparent spheres as a representation and demonstrates the expressive power of such primitive-based models. More recently, Gaussians were proposed as a primitive [9], and were shown to achieve both very high-quality image reconstruction and better than real-time inference speeds. This result sparked a significant number of follow-up works, ranging from modelling dynamic content [11, 28, 30, 32], to generative modelling [2, 27, 34]. There were also improvements made to the handling of primitive scale in rendering to avoid aliasing [29, 31].

**Depth guidance and regularization.** Other differentiable rendering works have also recognized the potential of depth regularization and supervision in improving novel view synthesis results. Works such as RegNeRF [21], LOLNeRF [23], and Mip-NeRF 360 [1] all proposed some form of regularization of the density sampled along a ray in order to improve the recovered 3D structure. Other works [5, 20, 24] have explored directly supervising depth to improve the final rendered results.

## 3. Method

Gaussian Splatting [9] represents scenes as collections of 3D Gaussian primitives, each associated with a mean  $\mu$ , covariance matrix  $\Sigma$ , opacity  $\alpha$  and RGB spherical harmonics coefficients  $h$ . These primitives can be used to render the scene by sequentially projecting the Gaussians in depth order into image space and rasterizing them with alpha blending to obtain a final color for each ray  $\mathbf{r}$ :

$$C_{GS}(\mathbf{r}) = \sum_{i=1}^N c(\mathbf{r}; h_i) \alpha_i \mathcal{G}(\mathbf{r}; \Sigma_i, \mu_i) \prod_{j=1}^{i-1} (1 - \alpha_j \mathcal{G}(\mathbf{r}; \Sigma_j, \mu_j)), \quad (1)$$

where  $c(\mathbf{r}; h)$  denotes querying the spherical color function in the direction of  $\mathbf{r}$ , and  $\mathcal{G}(\mathbf{r}; \Sigma, \mu)$  is the projection of the 3D Gaussian PDF into image space. Such a model is differentiable with respect to all parameters, and can therefore be trained by image reconstruction objectives. This, in theory, should allow continuous optimization starting from a random initialization, similar to NeRF.

However, unlike NeRF, the point-based nature of Gaussian Splatting models is less able to converge from a random initialization far from the final distribution of primitives. For this reason, the original Gaussian Splatting method employed discrete splitting, cloning, and pruning heuristics, which interrupt the continuous optimization to take larger



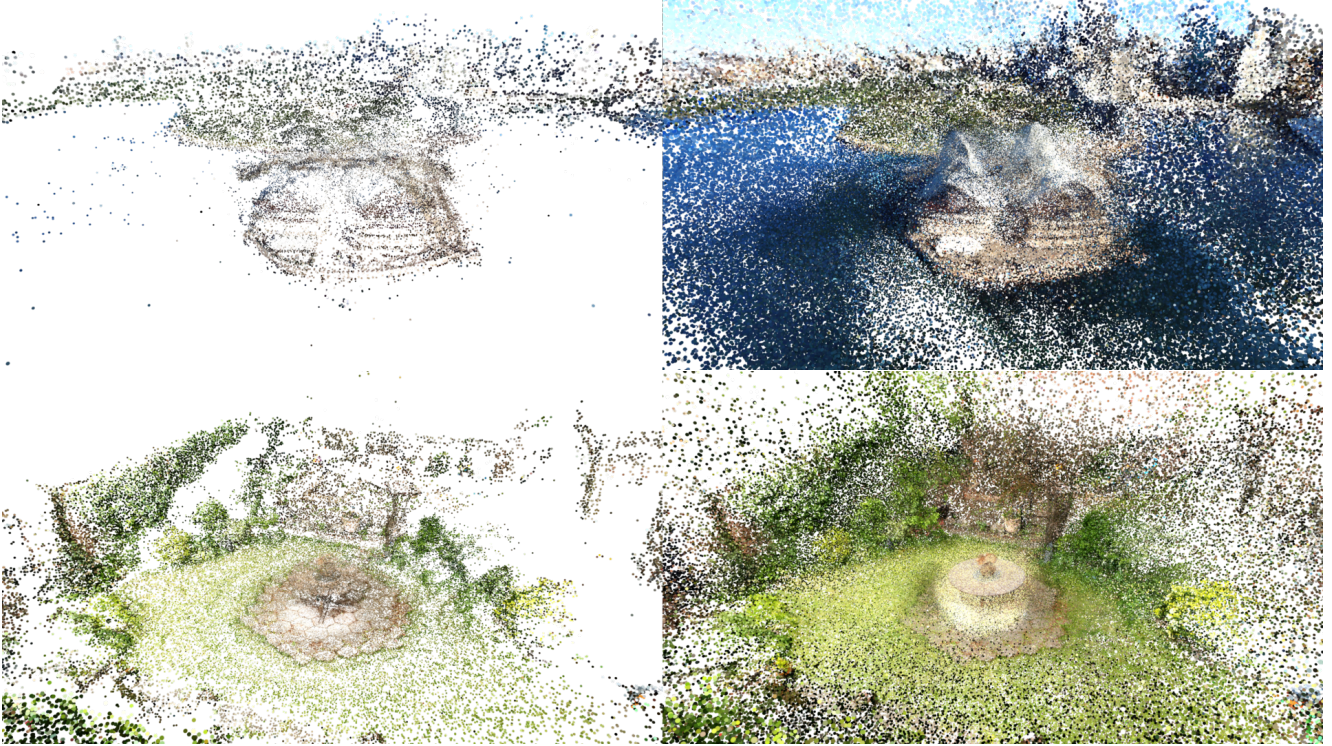


Figure 2. COLMAP (Left) vs. NeRF-based (Right) initialization point clouds for Gaussian Splatting. In this scene from OMMO [15] (Top), the surface of the water is dominated by dynamic content (waves), and view-dependent effects (reflections), which causes the SFM point cloud to be nearly empty in these areas. In contrast, the NeRF initialization is able to place points near this surface despite the lack of view-consistent detail. Even for more static and Lambertian scenes, such as the garden from Mip-NeRF 360 [1] (Bottom), the NeRF point cloud is still significantly more complete.

steps toward an optimal configuration, as defined by tuned thresholds. This approach is at least partially effective in closing the gap between Gaussian Splatting and NeRF in terms of scene structure recovery, but for large-scale, complex scenes, the original publication [9] still reported significant gains when initializing from an SFM point cloud versus a uniform random distribution.

In the remainder of this section, we will describe the potential strategies for closing this gap which we chose to evaluate.

### 3.1. Strategies for random initialization

The first and most obvious approach to avoiding the use of SFM initialization is to simply search for better random initializations which do not require knowledge of the scene structure. The experiments with random initialization performed in the original paper are described as using a uniform distribution of Gaussian centers within a scaled version of the camera bounding box. In our experiments, we attempt to reproduce the results of this bounding box strategy, as well as using an even simpler strategy of a very large uniform initialization sufficient to cover the entire scene. We report the results of these experiments in Section 4.2, as well as

comparison to the results reported in the original paper.

### 3.2. Initialization from a volumetric model

Beyond seeking an “improved” random initialization, we also look for ways that the superior structure recovery of volumetric NeRF models can be leveraged to bootstrap the training of Gaussian Splatting. We approach this by using a probabilistic interpretation of NeRF density in volume rendering which sees volume rendering weights as a distribution of “surface” locations, i.e. where a ray is likely to terminate [7]. This differential<sup>1</sup> “surfacedness” value at a depth  $t$  along some ray  $\mathbf{r}$  is defined as:

$$S(t; \mathbf{r}) = \sigma(\mathbf{r}(t)) \cdot \exp \left( - \int_{t_{\min}}^t \sigma(\mathbf{r}(s)) ds \right), \quad (2)$$

where  $\sigma(\mathbf{r}(t))$  denotes the NeRF density at depth  $t$  along  $\mathbf{r}$ . This termination probability can then be used to derive a cumulative distribution function along each ray:

$$W(t; \mathbf{r}) = \int_{t_{\min}}^t S(t; \mathbf{r}) ds. \quad (3)$$

<sup>1</sup>Note we use an unbounded differential value so as to define a continuous PDF, rather than integrating over a local interval as in [7].

Under this interpretation, the importance samples used in NeRF volume rendering can be repurposed as samples drawn from regions where the NeRF model “expects” the surface to be. We draw a set of such samples from a trained NeRF model, and use the spatial positions of these samples, along with the predicted NeRF radiance, to initialize a Gaussian Splatting model:

$$\mu = \mathbf{r}(W^{-1}(u; \mathbf{r})), \quad c = c_{\text{NeRF}}(\mu; \mathbf{r}), \quad u \sim \mathcal{U}[0, 1], \quad (4)$$

where  $W^{-1}(u; \mathbf{r})$  is the inverse CDF which maps the random parameter  $u$  to a depth along the ray  $\mathbf{r}$ , and  $c_{\text{NeRF}}(\mu; \mathbf{r})$  is the color value queried from the radiance field at the sample location  $\mu$  in the direction of  $\mathbf{r}$ . Given the large number of rays in each scene, we uniformly sample a subset of all training rays and draw a single sample from each ray.

**Implementation.** To keep our analysis as general as possible, we choose an efficient, off-the-shelf NeRF implementation, specifically NerfAcc [13], to base our experiments on. We use the proposal network-based INGP [18] model in NerfAcc, which supports large scale 360 degree scenes by implementing the scene contraction and proposal components of Mip-NeRF 360 [1]. We found this model to provide an excellent balance of flexibility and efficiency.

### 3.3. Volumetric structure distillation

In addition to simply initializing from the NeRF, we also investigated using depth prediction from the NeRF to guide training of the Gaussian Splatting model with an additional loss term. To do this, the rendering process for Gaussian Splatting must be modified to also predict depth values in a differentiable way. We use a similar formulation to the alpha compositing model for color rendering:

$$D_{\text{GS}}(\mathbf{r}) = \sum_{i=1}^N d_i \alpha_i \mathcal{G}(\mathbf{r}; \Sigma_i, \mu_i) \prod_{j=1}^{i-1} (1 - \alpha_j \mathcal{G}(\mathbf{r}; \Sigma_j, \mu_j)), \quad (5)$$

where  $d_i$  is the mean of the 1D Gaussian conditional distribution formed by the intersection of  $\mathbf{r}$  with the 3D Gaussian (see the Supplementary Material for derivation). Depth estimates can similarly be extracted from the NeRF model by accumulating sample depth:

$$D_{\text{NeRF}}(\mathbf{r}) = \int_{t_{\min}}^{t_{\max}} t \sigma(\mathbf{r}(t)) \exp\left(-\int_{t_{\min}}^t \sigma(\mathbf{r}(s)) ds\right) dt. \quad (6)$$

We precompute depth estimates from the NeRF model for all training rays, and incorporate them into the Gaussian Splatting term using the following loss:

$$\begin{aligned} \mathcal{L}_{\text{GS+Depth}} &= \mathcal{L}_{\text{GS}} + \lambda \mathcal{L}_{\text{Depth}}, \\ \mathcal{L}_{\text{Depth}} &= \mathbb{E}_{\mathbf{r}} \left[ |D_{\text{NeRF}}(\mathbf{r}) - D_{\text{GS}}(\mathbf{r})| \right], \end{aligned} \quad (7)$$

where  $\mathcal{L}_{\text{GS}}$  is the original Gaussian Splatting loss function, and  $\lambda$  is a weight which we schedule over training to control the strength of the structure guidance; see the Supplementary Material.

### 3.4. Hyper-parameters

The original Gaussian Splatting implementation depends on a number of parameters which are tuned based on the original photometric loss formulation. As such, it is necessary to take care in setting parameters when changing the loss formulation. We found through experimentation that including a depth term in the loss function alters the training dynamics of pruning, splitting and cloning, which can lead to an excessive number of Gaussians being instantiated if the wrong parameters are used. For all real data scenes, we use an exponential decay schedule for the depth loss weight  $\lambda$  with an initial value of 0.9, and a decay rate of 0.9 every 100 iterations. For synthetic scenes, we set the initial  $\lambda$  to 0.95 and the decay value to 0.8. We also observed better results by changing the start of densification to iteration 100 rather than 500.

## 4. Experiments

### 4.1. Datasets

To best evaluate how the strategies under consideration perform in real-world scenarios, we focus our experiments on large scale, outdoor datasets. The first dataset we employ is the Mip-NeRF 360 dataset [1], which includes several challenging indoor and outdoor scenes, and is a common benchmark for inverse rendering methods. We also evaluate on the OMMO dataset [15], which contains extremely large-scale scenes captured by drone videos. This is representative of an application area where eliminating reliance on SFM initialization would be advantageous, as autonomous vehicles often have accurate navigation systems that could be used as an alternative to purely visual tracking. These scenes also contain dynamic objects and strong view-dependence which degrade SFM point cloud coverage, as shown in Figure 2.

### 4.2. Analysis of random initialization

We start our analysis by taking a deeper look at the conclusions drawn about random initialization in the original Gaussian Splatting publication. Specifically, we try to *reproduce* the reported results for the original proposed method for uniform random initialization.

According to the original text, the authors “uniformly sample a cube with a size equal to three times the extent of the input camera’s bounding box” [9]. As shown in Table 1, we find this strategy to give higher PSNR values than originally reported, with the original values more closely matching those of a bounding box with  $1.5\times$  the extent of the cameras. However, we find an even simpler strategy of





Figure 3. Qualitative results on a scene from the Mip-NeRF 360 dataset [15]. We observe that the denser initialization from NeRF, and the structure guidance both lead to decreased loss of detail and thin geometry. Please zoom in to see details.

using a very large box centered at the origin without dependence on the camera distribution, covering a  $50 \times 50 \times 50$  extent in COLMAP coordinates (effectively covering the entire space) to give even better results in average, so we use this as our baseline random initialization going forward.

As also shown in Table 1, we also find that re-running the experiments with COLMAP initialization on the current official public code release results in *slightly better* results than originally reported. For all relevant experiments we provide both the original reported values as well as what we



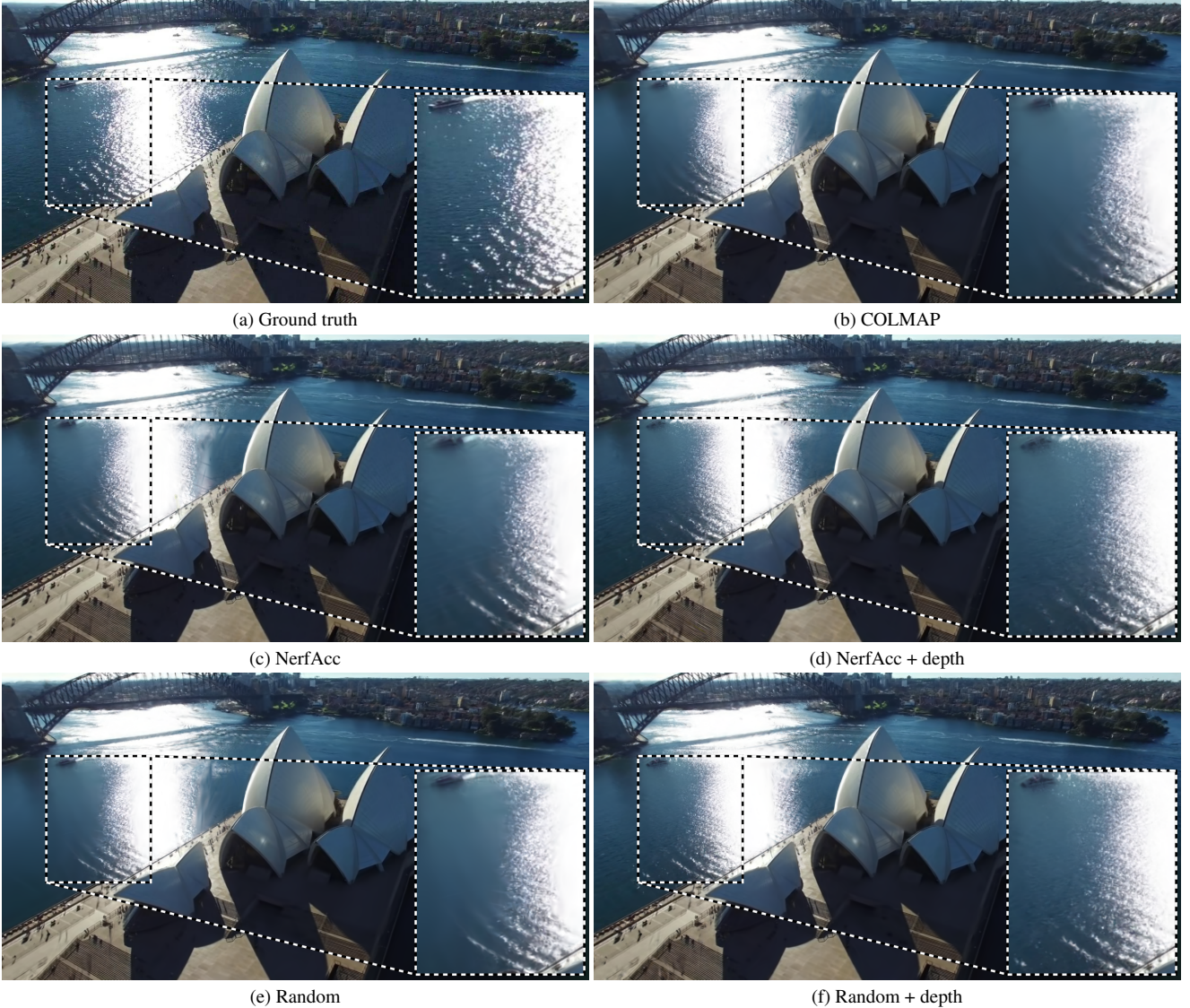


Figure 4. Qualitative results on a scene from the OMMO dataset [15]. We find that the COLMAP and random initializations allocate fewer points to the surface of the water, which leads to over-smoothed reconstruction compared to the NeRF-based initialization and models with depth supervision. Please zoom in to see details.

obtained re-running the code.

### 4.3. Volumetric vs. SFM initialization

With our baseline for random initialization selected, we move on to testing initialization based on a trained NeRF model. As described in Section 3.3, for each scene, we sample point cloud initializations consisting of 500,000 points in total from a NerfAcc-based INGP model trained to 5000, 10000, and 30000 iterations. These initializations are loaded in exactly the same way as COLMAP point clouds, and training proceeds with the same standard settings.

As reported in Tables 2 and 3, we find that these initializa-

tions near-universally outperform purely random initialization, and for some scenes outperform COLMAP initialization, even when using NeRF models trained for only 5000 iterations (about 30 seconds on our RTX 4090 GPU).

Based on these results, which show inconsistent improvement from training the initial NeRF model longer, we choose to proceed to the final round of experiments with the NeRF initializations from the 5000-iteration model weights, as this minimizes the additional compute added to the pipeline from NeRF pre-training.





(a) COLMAP Initialization



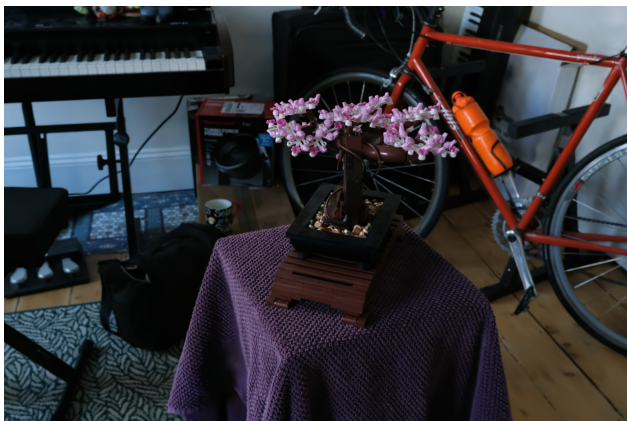
(b) Ours



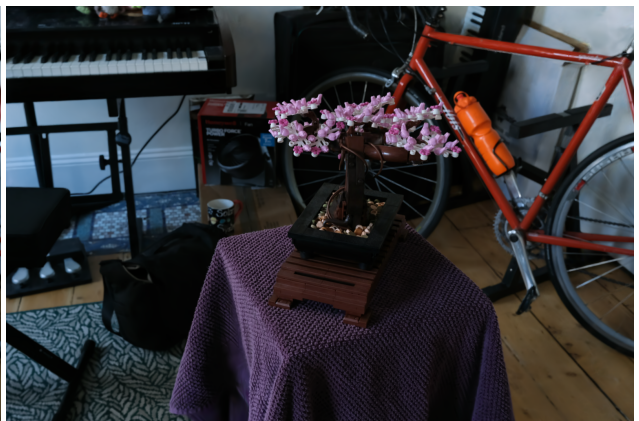
(c) COLMAP Initialization



(d) Ours



(e) COLMAP Initialization



(f) Ours



(g) COLMAP Initialization



(h) Ours

Figure 5. Additional qualitative results from the OMMO dataset [15] and Mip-NeRF 360. Here we visualize only the result of training with COLMAP (Left) and our best performing model with NeRF initialization + depth supervision (Right), to highlight the total contribution of the strategies we evaluated. Please zoom in to see details.





(a) NerfAcc



(b) Gaussian Splatting



(c) NerfAcc



(d) Gaussian Splatting



(e) NerfAcc



(f) Gaussian Splatting

Figure 6. Here we visualize the depth supervision from a NerfAcc model trained for 5000 iterations with the final depth rendered from the trained Gaussian Splatting model. The coarse structure of the NeRF depth is well-aligned with the final result, and allows Gaussian Splatting to more quickly refine the fine structures.

#### 4.4. Depth distillation from NeRF

Finally, we experiment with integrating direct depth guidance from the NeRF model into the Gaussian Splatting train-

ing pipeline (see Figure 6 for examples). Using the loss formulation in (7), we directly supervise predicted depth values from Gaussian Splatting with the pre-trained NeRF model, which enables more fine-grained transfer of structure.



Table 1. **Random initializations.** We compare test PSNR values for the Mip-NeRF 360 dataset [1] resulting from different random initialization schemes to the PSNR values obtained with COLMAP initialization. We both retrieve metrics from the original paper (From [9]), and re-run the official code release (re-run). We find that using a large constant  $50 \times 50 \times 50$  bounding box as the initialization gives the best results. All models are trained to the maximum 30k iterations used in the original paper, and all random initializations start with 50k Gaussians, which we found to perform well across scenes and random distributions.

Initialization	Scene							Average
	Garden	Bicycle	Stump	Counter	Kitchen	Bonsai	Room	
COLMAP (From [9])	27.41	25.25	26.55	28.70	30.32	31.98	30.63	28.69
COLMAP (Re-run)	27.29	25.16	26.82	29.19	31.50	32.25	31.43	29.09
$3 \times$ BBox (From [9])	22.19	21.05	-	-	-	-	-	-
$3 \times$ BBox (Re-run)	26.51	23.60	23.00	27.48	30.33	29.91	30.16	27.28
$1.5 \times$ BBox	22.03	21.28	20.71	25.04	26.15	17.15	29.69	23.15
$50^3$ BBox	26.31	24.12	24.63	28.04	30.54	30.74	29.90	27.75

Table 2. **Volumetric initialization (Mip-NeRF 360).** We evaluate test PSNR on the Mip-NeRF 360 dataset [1] when initializing the Gaussian Splatting model from INGP models trained for different amounts of time.

Initialization	Scene							Average
	Garden	Bicycle	Stump	Counter	Kitchen	Bonsai	Room	
COLMAP (From [9])	27.41	25.25	26.55	28.70	30.32	31.98	30.63	28.69
COLMAP (Re-run)	27.29	25.16	26.82	29.19	31.50	32.25	31.43	29.09
$50^3$ Random	26.31	24.12	24.63	28.04	30.54	30.74	29.90	27.75
NerfAcc @ 5k	27.21	23.90	27.35	28.47	31.82	31.88	32.11	28.96
NerfAcc @ 10k	27.29	24.14	27.37	28.77	31.97	32.27	32.01	29.12
NerfAcc @ 30k	27.28	24.11	27.38	28.50	31.71	31.78	31.93	28.96

Table 3. **Volumetric initialization (OMMO).** We evaluate test PSNR on the OMMO dataset [15] when initializing the Gaussian Splatting model from INGP models trained for different amounts of time.

Initialization	Scene							Average
	03	05	06	10	13	14	15	
COLMAP	26.07	28.36	26.76	29.72	32.55	31.11	30.46	29.29
$50^3$ Random	25.41	28.06	27.12	29.49	31.08	30.26	29.25	28.67
NerfAcc @ 5k	25.57	28.36	27.70	29.36	32.24	30.83	30.45	29.22
NerfAcc @ 10k	25.20	28.37	27.73	29.21	32.21	30.91	30.52	29.16
NerfAcc @ 30k	25.52	28.22	27.51	29.23	31.83	30.96	30.58	29.12

Table 4. **Structure distillation (Mip-NeRF 360)**. We evaluate test PSNR on the Mip-NeRF 360 dataset [1] when applying our depth loss for structure distillation from INGP models trained for 5k iterations.

Initialization	Scene							
	Garden	Bicycle	Stump	Counter	Kitchen	Bonsai	Room	Average
COLMAP (From [9])	27.41	25.25	26.55	28.70	30.32	31.98	30.63	28.69
COLMAP (Re-run)	27.29	25.16	26.82	29.19	31.50	32.25	31.43	29.09
NerfAcc @ 5k	27.21	23.90	27.35	28.47	31.82	31.88	32.11	28.96
50 <sup>3</sup> Random + Depth Loss	26.75	24.05	25.63	28.56	31.60	31.29	31.19	28.44
NerfAcc @ 5k + Depth Loss	27.37	25.22	27.21	28.85	31.87	31.54	31.63	29.10

Table 5. **Structure distillation (OMMO)**. We evaluate test PSNR on the OMMO dataset [15] when applying our depth loss for structure distillation from INGP models trained for 5k iterations.

Initialization	Scene							
	03	05	06	10	13	14	15	Average
COLMAP	26.07	28.36	26.76	29.72	32.55	31.11	30.46	29.29
NerfAcc @ 5k	25.57	28.36	27.70	29.36	32.24	30.83	30.45	29.22
50 <sup>3</sup> Random + Depth Loss	26.78	28.31	28.42	30.67	32.50	30.54	30.29	29.64
NerfAcc @ 5k + Depth Loss	26.48	28.50	28.89	30.54	32.74	31.07	30.76	29.85

It also helps avoid erroneous pruning of geometry as shown in Figure 3.

We report the results of these experiments in Tables 4 and 5, which show that the best final results are achieved with a combination of NeRF-based initialization and NeRF depth supervision.

We additionally check that our depth supervision strategy is not harmful in cases where standard Gaussian Splatting is already sufficient by testing it on the NeRF synthetic dataset [17]. This dataset is object-centric, with blank backgrounds, and performs well with only a random initialization to the bounding box of the object. As shown in Table 6, we

find that there is minimal difference in average between the depth-supervised and standard training on this dataset, suggesting that inclusion of depth distillation is not harmful in cases where it is not strictly necessary.

## 5. Conclusion

We performed an analysis of several approaches for avoiding SFM initialization in training of Gaussian Splatting. Through our experiments, we found that random initialization can perform better than expected based on the results of the original Gaussian Splatting paper. We also found that use of a small amount of time spent pre-training a NeRF model

Table 6. **Structure distillation (NeRF synthetic)**. We evaluate test PSNR on the NeRF synthetic dataset [17] when applying our depth loss for structure distillation from INGP models trained for 5k iterations.

Initialization	Scene							
	Lego	Ship	Hotdog	Materials	Ficus	Chair	Drums	Mic
Random (From [9])	35.78	30.81	37.72	30.00	34.87	35.83	26.15	35.36
Random (Re-run)	36.38	31.80	38.14	30.51	35.50	35.73	26.30	36.75
Random + Depth Loss	36.45	31.74	38.29	30.43	35.04	35.43	26.10	36.80

can enable results on par with or better than those achieved by COLMAP initialization by providing both a dense initial point cloud and depth supervision throughout training.

**Limitations.** The most immediate limitation in applying the strategies we have described to avoid requiring SFM solutions for Gaussian Splatting is that for many use cases, SFM is still the most reliable way of obtaining the camera calibration necessary to train. While our results suggest that there can still be value to leveraging NeRF pre-training when SFM points are available, it would be ideal to combine with other pipeline components capable of replacing SFM camera estimates.

Another potential complication to including these strategies in a robust pipeline is the NeRF training. While we found un-modified NerfAcc to perform well on Mip-NeRF 360 and OMMO, the default settings were not able to reconstruct the Tanks and Temples [10] scenes well enough to be useful for supervision. This suggests that more work might be needed to automate the NeRF configuration process to avoid adding to the tuning workload of the entire pipeline.

## References

- [1] Jonathan T Barron, Ben Mildenhall, Dor Verbin, Pratul P Srinivasan, and Peter Hedman. Mip-nerf 360: Unbounded anti-aliased neural radiance fields. In *Proceedings of the IEEE/CVF Conference on Computer Vision and Pattern Recognition*, pages 5470–5479, 2022. 2, 3, 4, 9, 10, 13, 14
- [2] David Charatan, Sizhe Li, Andrea Tagliasacchi, and Vincent Sitzmann. pixelsplat: 3d gaussian splats from image pairs for scalable generalizable 3d reconstruction. *arXiv preprint arXiv:2312.12337*, 2023. 2
- [3] Anpei Chen, Zexiang Xu, Andreas Geiger, Jingyi Yu, and Hao Su. Tensorf: Tensorial radiance fields. In *European Conference on Computer Vision*, pages 333–350. Springer, 2022. 2
- [4] Zhiqin Chen and Hao Zhang. Learning implicit fields for generative shape modeling. In *Proceedings of the IEEE/CVF Conference on Computer Vision and Pattern Recognition*, pages 5939–5948, 2019. 2
- [5] Kangle Deng, Andrew Liu, Jun-Yan Zhu, and Deva Ramanan. Depth-supervised nerf: Fewer views and faster training for free. In *Proceedings of the IEEE/CVF Conference on Computer Vision and Pattern Recognition*, pages 12882–12891, 2022. 2
- [6] Sara Fridovich-Keil, Alex Yu, Matthew Tancik, Qinhong Chen, Benjamin Recht, and Angjoo Kanazawa. Plenoxels: Radiance fields without neural networks. In *Proceedings of the IEEE/CVF Conference on Computer Vision and Pattern Recognition*, pages 5501–5510, 2022. 2
- [7] Lily Goli, Daniel Rebain, Sara Sabour, Animesh Garg, and Andrea Tagliasacchi. nerf2nerf: Pairwise registration of neural radiance fields. In *International Conference on Robotics and Automation (ICRA)*. IEEE, 2023. 3
- [8] Peter Hedman, Julien Philip, True Price, Jan-Michael Frahm, George Drettakis, and Gabriel Brostow. Deep blending for free-viewpoint image-based rendering. *ACM Transactions on Graphics (ToG)*, 37(6):1–15, 2018. 13
- [9] Bernhard Kerbl, Georgios Kopanas, Thomas Leimkühler, and George Drettakis. 3d gaussian splatting for real-time radiance field rendering. *ACM Transactions on Graphics*, 42(4), 2023. 1, 2, 3, 4, 9, 10, 13, 14
- [10] Arno Knapitsch, Jaesik Park, Qian-Yi Zhou, and Vladlen Koltun. Tanks and temples: Benchmarking large-scale scene reconstruction. *TOG*, 2017. 11, 13
- [11] Muhammed Kocabas, Jen-Hao Rick Chang, James Gabriel, Oncel Tuzel, and Anurag Ranjan. Hugs: Human gaussian splats. *arXiv preprint arXiv:2311.17910*, 2023. 2
- [12] Christoph Lassner and Michael Zollhofer. Pulsar: Efficient sphere-based neural rendering. In *Proceedings of the IEEE/CVF Conference on Computer Vision and Pattern Recognition*, pages 1440–1449, 2021. 2
- [13] Ruilong Li, Hang Gao, Matthew Tancik, and Angjoo Kanazawa. Nerfacc: Efficient sampling accelerates nerfs. *arXiv preprint arXiv:2305.04966*, 2023. 4
- [14] Lingjie Liu, Jiatao Gu, Kyaw Zaw Lin, Tat-Seng Chua, and Christian Theobalt. Neural sparse voxel fields. *Advances in Neural Information Processing Systems*, 33:15651–15663, 2020. 2
- [15] Chongshan Lu, Fukun Yin, Xin Chen, Tao Chen, Gang Yu, and Jiayuan Fan. A large-scale outdoor multi-modal dataset and benchmark for novel view synthesis and implicit scene reconstruction. *arXiv preprint arXiv:2301.06782*, 2023. 3, 4, 5, 6, 7, 9, 10, 13, 14
- [16] Lars Mescheder, Michael Oechsle, Michael Niemeyer, Sebastian Nowozin, and Andreas Geiger. Occupancy networks: Learning 3d reconstruction in function space. In *Proceedings of the IEEE/CVF conference on computer vision and pattern recognition*, pages 4460–4470, 2019. 2
- [17] Ben Mildenhall, Pratul P Srinivasan, Matthew Tancik, Jonathan T Barron, Ravi Ramamoorthi, and Ren Ng. Nerf: Representing scenes as neural radiance fields for view synthesis. *Communications of the ACM*, 65(1):99–106, 2021. 1, 2, 10
- [18] Thomas Müller, Alex Evans, Christoph Schied, and Alexander Keller. Instant neural graphics primitives with a multiresolution hash encoding. *ACM Trans. Graph.*, 41(4):102:1–102:15, 2022. 2, 4
- [19] Raul Mur-Artal, Jose Maria Martinez Montiel, and Juan D Tardos. Orb-slam: a versatile and accurate monocular slam system. *IEEE transactions on robotics*, 31(5):1147–1163, 2015. 1
- [20] Thomas Neff, Pascal Stadlbauer, Mathias Parger, Andreas Kurz, Joerg H. Mueller, Chakravarty R. Alla Chaitanya, Anton S. Kaplanyan, and Markus Steinberger. DONeRF: Towards Real-Time Rendering of Compact Neural Radiance Fields using Depth Oracle Networks. *Computer Graphics Forum*, 2021. 2
- [21] Michael Niemeyer, Jonathan T. Barron, Ben Mildenhall, Mehdi S. M. Sajjadi, Andreas Geiger, and Noha Radwan. Regnerf: Regularizing neural radiance fields for view synthesis from sparse inputs. In *Proc. IEEE Conf. on Computer Vision and Pattern Recognition (CVPR)*, 2022. 2



- [22] Jeong Joon Park, Peter Florence, Julian Straub, Richard Newcombe, and Steven Lovegrove. DeepSDF: Learning continuous signed distance functions for shape representation. In *Proceedings of the IEEE/CVF conference on computer vision and pattern recognition*, pages 165–174, 2019. 2
- [23] Daniel Rebain, Mark Matthews, Kwang Moo Yi, Dmitry Lagun, and Andrea Tagliasacchi. LoloNet: Learn from one look. In *Proceedings of the IEEE/CVF Conference on Computer Vision and Pattern Recognition*, pages 1558–1567, 2022. 2
- [24] Barbara Roessle, Jonathan T Barron, Ben Mildenhall, Pratul P Srinivasan, and Matthias Nießner. Dense depth priors for neural radiance fields from sparse input views. In *Proceedings of the IEEE/CVF Conference on Computer Vision and Pattern Recognition*, pages 12892–12901, 2022. 2
- [25] Johannes Lutz Schönberger and Jan-Michael Frahm. Structure-from-motion revisited. In *Conference on Computer Vision and Pattern Recognition (CVPR)*, 2016. 1
- [26] Johannes Lutz Schönberger, Enliang Zheng, Marc Pollefeys, and Jan-Michael Frahm. Pixelwise view selection for unstructured multi-view stereo. In *European Conference on Computer Vision (ECCV)*, 2016. 1
- [27] Jiaxiang Tang, Jiawei Ren, Hang Zhou, Ziwei Liu, and Gang Zeng. Dreamgaussian: Generative gaussian splatting for efficient 3d content creation. *arXiv preprint arXiv:2309.16653*, 2023. 2
- [28] GuanJun Wu, Taoran Yi, Jiemin Fang, Lingxi Xie, Xiaopeng Zhang, Wei Wei, Wenyu Liu, Qi Tian, and Xinggang Wang. 4d gaussian splatting for real-time dynamic scene rendering. *arXiv preprint arXiv:2310.08528*, 2023. 2
- [29] Zhiwen Yan, Weng Fei Low, Yu Chen, and Gim Hee Lee. Multi-scale 3d gaussian splatting for anti-aliased rendering. *arXiv preprint arXiv:2311.17089*, 2023. 2
- [30] Ziyi Yang, Xinyu Gao, Wen Zhou, Shaohui Jiao, Yuqing Zhang, and Xiaogang Jin. Deformable 3d gaussians for high-fidelity monocular dynamic scene reconstruction. *arXiv preprint arXiv:2309.13101*, 2023. 2
- [31] Zehao Yu, Anpei Chen, Binbin Huang, Torsten Sattler, and Andreas Geiger. Mip-splatting: Alias-free 3d gaussian splatting. *arXiv preprint arXiv:2311.16493*, 2023. 2
- [32] Ye Yuan, Xueting Li, Yangyi Huang, Shalini De Mello, Koki Nagano, Jan Kautz, and Umar Iqbal. GAvatar: Animatable 3d gaussian avatars with implicit mesh learning. *arXiv preprint arXiv:2312.11461*, 2023. 2
- [33] Richard Zhang, Phillip Isola, Alexei A Efros, Eli Shechtman, and Oliver Wang. The unreasonable effectiveness of deep features as a perceptual metric. In *CVPR*, 2018. 13
- [34] Zi-Xin Zou, Zhipeng Yu, Yuan-Chen Guo, Yangguang Li, Ding Liang, Yan-Pei Cao, and Song-Hai Zhang. Triplane meets gaussian splatting: Fast and generalizable single-view 3d reconstruction with transformers. *arXiv preprint arXiv:2312.09147*, 2023. 2

Table 7. **Results on the Deep Blending dataset [8]**. We report metrics (PSNR / SSIM / LPIPS) on the two Deep Blending scenes reported in Gaussian Splatting.

Initialization	Scene		
	DrJohnson	Playroom	Average
COLMAP (From [9])	28.77 / <b>0.8990</b> / 0.2440	30.04 / <b>0.9060</b> / 0.2410	29.41 / <b>0.9025</b> / 0.2425
COLMAP (Re-run)	29.85 / 0.8946 / 0.1585	28.96 / 0.8876 / 0.1774	29.41 / 0.8911 / 0.1680
NerfAcc @ 5k	30.33 / 0.8962 / <b>0.1530</b>	29.41 / 0.8929 / <b>0.1707</b>	29.87 / 0.8946 / <b>0.1618</b>
50 <sup>3</sup> Random + Depth Loss	29.92 / 0.8874 / 0.1628	29.10 / 0.8863 / 0.1838	29.51 / 0.8868 / 0.1733
NerfAcc @ 5k + Depth Loss	29.90 / 0.8883 / 0.1581	29.54 / 0.8929 / 0.1717	29.72 / 0.8906 / 0.1649

Table 8. **SSIM on the Mip-NeRF 360 dataset [1]**. We report SSIM metric on the Mip-NeRF 360 scenes reported in Gaussian Splatting.

Initialization	Scene							
	Garden	Bicycle	Stump	Counter	Kitchen	Bonsai	Room	Average
COLMAP (From [9])	0.8680	0.7710	0.7750	0.9050	0.9220	0.9380	0.9140	0.8704
COLMAP (Re-run)	0.8598	0.7517	0.7669	0.9085	0.9312	0.9423	0.9227	0.8690
NerfAcc @ 5k	0.8598	0.7723	0.7927	0.9042	0.9325	0.9436	0.9253	0.8758
50 <sup>3</sup> Random + Depth Loss	0.8433	0.7010	0.7348	0.8863	0.9262	0.9385	0.9075	0.8482
NerfAcc @ 5k + Depth Loss	0.8622	0.7656	0.7927	0.9026	0.9334	0.9415	0.9220	0.8743

## A. Appendix Section

### A.1. Results on additional data

We repeat our experiments with NeRF-based initialization and depth distillation on two scenes from the Deep Blending dataset [8] which were used in the original Gaussian Splatting paper. These results are shown in Table 7, and also show that better initialization and depth distillation improve over the results from COLMAP initialization.

We also attempted to train Gaussian Splatting models for the “truck” and “train” scenes from the Tanks and Temples dataset [10], but were unable to find an unbounded INGP model which trained well enough for them to provide structure guidance. We did however observe that a better random initialization also outperformed the originally reported Gaussian Splatting results for these scenes, as we found with other datasets.

### A.2. Additional metrics

We additionally report the perceptual quality metrics SSIM and LPIPS [33] for the Mip-NeRF 360 [1] and OMMO [15] datasets. These results can be found in Tables 8, 9, 10, and 11.

### A.3. Additional qualitative results

Please see `index.html` for additional qualitative renders of test images.

### A.4. Depth rendering with Gaussians

To determine the depth of a Gaussian along a ray, we begin with the 3D Gaussian equation:

$$G(x) = \exp\left(-\frac{1}{2}x^T\Sigma^{-1}x\right), \quad (8)$$

where, without loss of generality, we neglect the mean  $\mu$  by assuming our coordinate system to be centered at  $\mu$ . We also ignore any normalization or weighting of the Gaussian, which will not impact its depth.

We begin the derivation by substituting  $o+td$  for  $x$ , where  $o$  and  $d$  are the origin and direction of the ray, and  $t$  is the depth:

$$G(x) = \exp\left(-\frac{1}{2}(o+td)^T\Sigma^{-1}(o+td)\right). \quad (9)$$

By expanding the polynomial, we can rewrite this as:

$$G(x) = \exp\left(-\frac{1}{2}(o^T\Sigma^{-1}o + 2td^T\Sigma^{-1}o + t^2d^T\Sigma^{-1}d)\right). \quad (10)$$

Table 9. **SSIM on the OMMO dataset [15]**. We report SSIM metric on the OMMO dataset containing large-scale scenes.

Initialization	Scene							Average
	03	05	06	10	13	14	15	
COLMAP	0.8642	0.8635	0.9018	0.8845	0.9446	0.9393	0.9304	0.9040
NerfAcc @ 5k	0.8657	0.8627	0.9083	0.8646	0.9262	0.9381	0.9320	0.8997
50 <sup>3</sup> Random + Depth Loss	0.8755	0.8615	0.9137	0.8858	0.9292	0.9358	0.9262	0.9040
NerfAcc @ 5k + Depth Loss	0.8849	0.8642	0.9220	0.8810	0.9344	0.9408	0.9362	0.9091

Table 10. **LPIPS on the Mip-NeRF 360 dataset [1]**. We report LPIPS metric on the Mip-NeRF 360 scenes reported in Gaussian Splatting.

Initialization	Scene							Average
	Garden	Bicycle	Stump	Counter	Kitchen	Bonsai	Room	
COLMAP (From [9])	0.1030	0.2050	0.2100	0.2040	0.1290	0.2050	0.2200	0.1823
COLMAP (Re-run)	0.0865	0.1957	0.1718	0.1439	0.0878	0.1175	0.1533	0.1366
NerfAcc @ 5k	0.0869	0.1722	0.1466	0.1458	0.0845	0.1131	0.1473	0.1281
50 <sup>3</sup> Random + Depth Loss	0.1057	0.2087	0.1796	0.1764	0.0955	0.1203	0.1852	0.1531
NerfAcc @ 5k + Depth Loss	0.0868	0.1809	0.1466	0.1446	0.0839	0.1110	0.1536	0.1296

To find the depth with the maximum Gaussian value along the ray, we can factor out the scale of the polynomial solve the argmin:

$$d = \arg \min_t \frac{o^T \Sigma^{-1} o}{d^T \Sigma^{-1} d} + 2t \frac{d^T \Sigma^{-1} o}{d^T \Sigma^{-1} d} + t^2, \quad (11)$$

$$d = -\frac{d^T \Sigma^{-1} o}{d^T \Sigma^{-1} d}. \quad (12)$$

### A.5. Scheduling of depth loss weight

We use the following schedule for the loss weight  $\lambda$ :

$$\lambda(i) = \lambda_{init} \times d^{\frac{i}{S}}, \quad (13)$$

where  $\lambda_{init}$  denotes initial weight,  $d$  and  $S$  represent decay rate and step, respectively and  $i$  stands for iteration.

Table 11. **LPIPS on the OMMO dataset [15]**. We report LPIPS metric on the OMMO dataset containing large-scale scenes.

Initialization	Scene							Average
	03	05	06	10	13	14	15	
COLMAP	0.1681	0.1930	0.1586	0.1678	0.0982	0.0755	0.0807	0.1346
NerfAcc @ 5k	0.1667	0.1682	0.1535	0.2015	0.1331	0.0783	0.0784	0.1399
50 <sup>3</sup> Random + Depth Loss	0.1530	0.1528	0.1348	0.1465	0.1324	0.0830	0.0873	0.1271
NerfAcc @ 5k + Depth Loss	0.1390	0.1368	0.1181	0.1601	0.1207	0.0742	0.0709	0.1171